Ion size influence on the Ar solvation shells of M +−C 6F 6 clusters (M = Na, K, Rb, Cs)

ARTICLE *in* THE JOURNAL OF PHYSICAL CHEMISTRY A · MARCH 2012

Impact Factor: 2.69 · DOI: 10.1021/jp300156k

2 AUTHORS:

Margarita Albertí Wirsing
University of Barcelona
91 PUBLICATIONS **939** CITATIONS
SEE PROFILE

Noelia Faginas Lago
Università degli Studi di Perugia
48 PUBLICATIONS **250** CITATIONS
SEE PROFILE

THE JOURNAL OF PHYSICAL CHEMISTRY A

Article

pubs.acs.org/JPCA

Ion Size Influence on the Ar Solvation Shells of $M^+-C_6F_6$ Clusters (M = Na, K, Rb, Cs)

M. Albertí*,† and N. Faginas Lago‡

†IQTCUB, Departament de Química Física, Universitat de Barcelona, Barcelona, Spain

‡Dipartimento di Chimica, Università di Perugia, Perugia, Italy

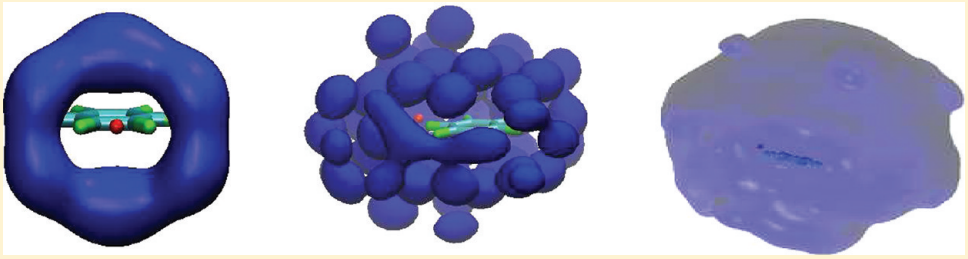

ABSTRACT: The size-specific influence of alkali metal ions in the gradual transition from cluster rearrangement to solvation dynamics is investigated by means of molecular dynamics simulations for alkali metal cation−hexafluorobenzene systems, $M^+-C_6F_6$ (M = Na, K, Rb and Cs), surrounded by Ar atoms. To analyze such transition, different small aggregates of the $M^+-C_6F_6-Ar_n$ (n = 1, ..., 30) type and $M^+-C_6F_6$ clusters solvated by about 500 Ar atoms are considered. The $Ar-C_6F_6$ interaction contribution has been described using two different formalisms, based on the interaction decomposition in atom−bond and in atom−effective atom terms, which have been applied to study the small aggregates and to investigate the Ar solvated $M^+-C_6F_6$ clusters, respectively. The selectivity of the promoted phenomena from the M^+ ion size and their dependence from the number of Ar atoms is characterized.

1. INTRODUCTION

Intermolecular interactions involving ions and aromatic rings play a key role in several chemical and biological processes, as for instance in molecular recognition and to rationally designing drugs,[1,2] for which the understanding of the physical origin of such interactions is essential. Several studies of the aromatic rings forming aggregates with both cations and anions can be found in the literature.[3−10] In particular, cation−π interactions, due to their importance for the understanding of biological structures,[11] for the selectivity of ionic channels,[12] and for the key role played in molecular recognition,[11,13] have been widely investigated.

The substitution of hydrogen atoms of benzene by electron withdrawing groups changes the nature of the charge cloud of the aromatic ring, allowing the study of the anion−π interaction nature, which plays an additional and important role in the molecular recognition of anions.[14−24] As a matter of fact, ions interacting with benzene (C_6H_6) and hexafluorobenzene (C_6F_6) can be considered as prototypical systems to investigate cation−π and anion−π interactions. C_6H_6 and C_6F_6, which have quadrupole moments comparable in magnitude but opposite in sign,[25] interact with the same ions forming completely different aggregates.[26] In particular, the alkali metal cations tend to tie C_6F_6 rings in a sheet whereas they tend to tie the C_6H_6 ones in a pile.[27,28] On the contrary, halides tend to tie C_6F_6 and C_6H_6 rings in a pile and in a sheet, respectively. Similarities and differences between cation−π and anion−π interactions have been also investigated.[29−32] Moreover, size-specific interactions of alkali metal ions with aromatic side chains have been proposed as a mechanism for selectivity in some K^+ channel proteins.[33] Accordingly, the modeling of intermolecular interactions in systems containing aromatic compounds and alkali metal ions can be very useful to model biological channels. As indicated above, the understanding of interactions between aromatic molecules and ions is crucial for both molecular recognition and designing drugs, for which solvation effects can also play a key role. Therefore, the solvation structure and dynamics of ions can selectively affect the behavior of many chemical and biological systems.[34,35]

In spite of the great effort invested in the experimental characterization of solvation,[34−37] the microscopic details of the solvation of ions are still not fully understood. The study of clusters formed by a solute molecule embedded in a flexible cage of solvent atoms (or molecules), as for instance an aromatic molecule in a well-characterized distribution of rare gas atoms,[38,39] has been recognized as a powerful tool to investigate in detail the process of solvation.[40−42] Accordingly, molecular dynamics (MD) simulations can be a useful complement to experimental results. However, one should think that the reliability of the predictions largely depends on the accuracy of the force field, which usually is described by means of analytical functions that need to be carefully tested by

Received: January 5, 2012
Revised: February 23, 2012
Published: February 29, 2012

comparing predictions with high level experimental data and/or ab initio results.

In the last years, we have devoted particular attention to MD simulations of the Ar solvation of $M^+-C_6H_6$ (M = Na, K, Rb, Cs)[43,44] and of $X^--C_6H_6$ (X = Cl, Br, I).[42,45,46] The comparison of $M^+-C_6H_6$ and $X^--C_6H_6$ when solvated by Ar atoms allowed us to analyze different aspects of the solvation processes, which were also investigated for the $Na^+-C_6H_6-Cl^-$ clusters.[47] In general, solvation processes are characterized by the particular structure of the solvent around the solute, which differs from that of pure solvent. The solvent structure, in the vicinity of the solute, can be strongly affected by the most stable structure of the unsolvated system.[47] In spite of this, differences on the solvation shells surrounding similar structures of different compounds can be observed. For instance, both $K^+-C_6F_6$ and $Cl^-C_6H_6$ form equilibrium on plane bifurcated structures; however, due to the different strength of the ion−Ar interactions, $K^+-C_6F_6-Ar$ is more stable than $Cl^-C_6H_6-Ar$. The lower Cl^-−Ar interaction energy, in comparison with the K^+−Ar one, originates differences on the $K^+-C_6F_6-Ar_n$ and the $Cl^-C_6H_6-Ar_n$ aggregates,[48] which are also evident when the number of Ar atoms increases. Accordingly, noticeable differences on the Ar solvation shells of $K^+-C_6F_6$ and $Cl^-C_6H_6$ are observed. Bearing in mind that both the geometry of the unsolvated system and the strength of the interaction energy contributions determine the main characteristics of the solvation shells, it seems interesting to further investigate the solvation processes of the $M^+-C_6F_6$ aggregates by analyzing in detail the differences with the solvation of $X^-C_6H_6$ (X = Cl, Br, I).[46] Moreover, the effect of the cation size, affecting both the interaction between the different partners and the geometry of the unsolvated system, adds interest to the study of the solvation of the $M^+-C_6F_6$ aggregates.

In the present paper, the microsolvation characteristics of the $M^+-C_6F_6$ (M = Na, K, Rb, Cs) aggregates are investigated. In section 2, the formulation of the potential energy function is outlined. The static properties of the $M^+-C_6F_6-Ar$ systems are given in section 3 and in section 4 the MD simulation results are presented. In section 5, the main conclusions are given.

2. INTERMOLECULAR INTERACTIONS IN THE Ar SOLVATED $M^+-C_6F_6$ AGGREGATES

Due to the different nature of the intermolecular interactions, often the total potential energy (V_{total}) is decomposed as sum of electrostatic (V_{el}) and nonelectrostatic (V_{nel}) contributions. For the $M^+-C_6F_6$ systems, V_{el} asymptotically is of the cation−quadrupole type and arises from the interaction between the cation charge and the charges assigned to the molecular frame. Thereby, V_{el} is often described as combination of Coulomb interactions between the electrostatic charge of the cation, equal to 1 au, and any punctual charge assigned to the molecular frame. Indeed, the distribution of the punctual charges must asymptotically reproduce the C_6F_6 quadrupole moment. In our simulations we have used charges of −0.12 au on each F atoms and two positive charges of 0.06 au separated by 0.137 Å assigned to each C atom and placed above and below the aromatic plane.[26] V_{nel} results from the balancing of both dispersion and induction attraction, dominant at long-range, with exchange (size) repulsion, dominant at short-range, and it is described by considering that the polarizability of the interaction partners is the key property to scale attraction and repulsion in systems involving noncovalent interactions.[49] In the present study, the molecular polarizability of C_6F_6 has been decomposed in two different ways: (1) bond polarizabilities (see, for instance, ref 50) and (2) atom effective polarizabilities (see, for instance, ref 48). In the first decomposition, each bond is identified with an ellipsoid of electric charge with an assigned value of the polarizability, whereas in the second, only used to represent the $Ar-C_6F_6$ interaction energy in the more complex systems, i.e., in those systems containing more than 30 Ar atoms, each bond polarizability is further decomposed in effective polarizabilities associated to the atoms forming the molecule. In both cases, the sum of the polarizability fragments is compatible with the value of the molecular polarizability.

Independently of the number of Ar atoms, V_{nel} is given as a combination of independent nonelectrostatic $M^+-C_6F_6$, $Ar-C_6F_6$, and $Ar-M^+$ energy contributions. Accordingly with the decomposition of the molecular polarizability used to investigate the smaller $M^+-C_6F_6-Ar_n$ ($n \leq 30$) aggregates, the $M^+-C_6F_6$ and the $Ar-C_6F_6$ energies are obtained as a sum of ion−bond (M^+−CC and M^+−CF) and atom−bond (Ar−CC and Ar−CF) contributions, respectively. In this case ($n \leq 30$) V_{nel} is then represented as

$$V_{nel} = \sum_{i=1}^{6} (V_{M^+-(CC)_i} + V_{M^+-(CF)_i}) + \sum_{i=1}^{6}\sum_{j=1}^{n} (V_{Ar_j-(CC)_i} + V_{Ar_j-(CF)_i}) + \sum_{j=1}^{n} V_{Ar_j-M^+} + \sum_{j=1}^{n-1}\sum_{k>j}^{n} V_{Ar_j-Ar_k} \quad (1)$$

Each ion(atom)−bond term is defined by assuming interaction centers placed on the ion(atom) and on the center of the considered bond.

For aggregates with $n > 30$, the $M^+-C_6F_6$ and $Ar-M^+$ are described in the same way as for the smaller aggregates, whereas the $Ar-C_6F_6$ energy, because of its more extended role, is calculated by a sum of atom−effective atom ($Ar-C_{eff}$ and $Ar-F_{eff}$) contributions. In this case ($n > 30$) V_{nel} is then represented as

$$V_{nel} = \sum_{i=1}^{6} (V_{M^+-(CC)_i} + V_{M^+-(CF)_i}) + \sum_{i=1}^{6}\sum_{j=1}^{n} (V_{Ar_j-(C_{eff})_i} + V_{Ar_j-(F_{eff})_i}) + \sum_{j=1}^{n} V_{Ar_j-M^+} + \sum_{j=1}^{n-1}\sum_{k>j}^{n} V_{Ar_j-Ar_k} \quad (2)$$

Each atom−effective atom term is defined by assuming interaction centers placed on the Ar atom and on each atom of C_6F_6.

dx.doi.org/10.1021/jp300156k | J. Phys. Chem. A 2012, 116, 3094−3102

All terms in eqs 1 and 2 are expressed by means of an improved Lennard-Jones function (ILJ),[51,52] whose general form is

$$V_{ILJ} = \varepsilon\left[\frac{m}{\beta + 4.0\left(\frac{r}{r_0}\right)^2 - m}\left(\frac{r_0}{r}\right)^{\beta+4.0(r/r_0)^2} - \frac{\beta + 4.0\left(\frac{r}{r_0}\right)^2}{\beta + 4.0\left(\frac{r}{r_0}\right)^2 - m}\left(\frac{r_0}{r}\right)^m\right] \quad (3)$$

In eq 3, ε and r_0 have identical meaning that in the traditional Lennard-Jones (LJ) model, namely depth of the potential well and its location. However, the ILJ function, thanks to the additional shape parameter β, assumes asymptotically a more realistic behavior with respect to LJ. Moreover, ε and r_0, considered the most relevant parameters of the potential, are transferable (the only not directly transferable parameter in eq 3 is β).[53] The m parameter has been taken equal to 4 and to 6 for ion-neutral and neutral-neutral interactions, respectively. The meaning of the distance variable r changes from the atom−bond to the atom−effective atom formalisms. In the first formalism, r represents the distance from Ar to the center of a given bond, whereas, in the second one, it represents the distance from Ar to the C and F atoms of the molecule.

The additivity of the bond ellipsoids and the decomposition of the associated mean polarizability in values along (parallel) and at right (perpendicular) angles to the bond were confirmed in the past.[54] In particular, these studies confirmed the availability of the interaction decomposition in atom−bond terms (three body terms). Accordingly, following such decomposition ε and r_0 in eq 3 are obtained by properly combining their perpendicular and parallel components, which for $M^+-C_6F_6-Ar_n$ are derived from the CC, CF, M^+, and Ar polarizabilities.[26,47,48] These potential parameters are given in Table 1. However, three-body potentials scale as N^3, where N is the number of particles, and MD programs usually apply no long-range corrections to the three body potentials. These facts suggest the use of simpler potentials than the three-body ones when the number of particles increases. Accordingly, for the larger systems, the interactions in which Ar is involved are described, by means of pair potentials and the usual atom−bond formulation of the C_6F_6−Ar interaction (exploiting Ar−CC and Ar−CF pair potentials) has been substituted by the atom−effective atom (Ar−C_{eff} and Ar−F_{eff}) one. This choice, motivated by the large number of Ar atoms considered, can be justified by taking into account the less direct role of the bond polarizability tensors on the basic features of neutral−neutral interactions compared to those of the ion neutral ones. However, the new atom−atom parameters (Table 2) have been selected to reproduce the main characteristics provided by the atom−bond formulation of the C_6F_6−Ar interaction. It must be stressed here that the formulation of V_{nel}, based on different decompositions of the molecular polarizability, has been widely tested by comparing several system predictions with accurate ab initio calculations[10,22,53,55,56] and high level experimental data.[52]

Table 1. Perpendicular and Parallel Components of the Well Depth ($\varepsilon_\perp$, $\varepsilon_\parallel$) and of the Equilibrium Distances ($r_{0\perp}$, $r_{0\parallel}$) for the Different Ion−Bond Pairs (M^+−CC, M^+−CF, Ar−CC, and Ar−CF)[a]

ion−bond	$\varepsilon_\perp$/meV	$\varepsilon_\parallel$/meV	$r_{0\perp}$/Å	$r_{0\parallel}$/Å	β
Na^+−CC	33.01	102.20	2.848	3.149	8.5
Na^+−CF	58.32	65.71	2.631	2.947	8.5
K^+−CC	22.95	75.77	3.266	3.547	8.5
K^+−CF	37.75	46.60	3.074	3.365	8.5
Rb^+−CC	20.52	69.77	3.435	3.705	8.5
Rb^+−CF	32.65	41.84	3.256	3.534	8.5
Cs^+−CC	18.20	64.11	3.638	3.894	8.5
Cs^+−CF	27.81	37.12	3.476	3.739	8.5
Ar−CC	3.895	4.910	3.879	4.189	9.0
Ar−CF	6.290	5.239	3.674	3.983	9.0

[a]The values of the β parameter are also given.

Table 2. Well Depth (ε) and Equilibrium Distances (r_0) for the M^+−Ar, Ar−Ar, Ar−C_{eff}, and Ar−F_{eff} Interactions[a]

ion(atom)−atom	ε/meV	r_0/Å	β
Na^+−Ar	167.00	2.730	9.0
K^+−Ar	110.00	3.190	8.9
Rb^+−Ar	97.00	3.360	8.2
Cs^+−Ar	85.00	3.570	8.0
Ar−Ar	12.37	3.757	9.0
Ar−C_{eff}	6.000	3.944	9.0
Ar−F_{eff}	6.152	3.550	9.0

[a]Ar−C_{eff} and Ar−F_{eff} Describe Ar−C_6F_6 Interactions for $n > 30$. The values of the β parameter are also given.

3. $M^+-C_6F_6$−Ar AGGREGATES

In this section the static properties of the $M^+-C_6F_6$−Ar aggregates are obtained as a function of the ion mass. In particular, our interest deals in analyzing both the structure and the energy at equilibrium. To this end, the distance from both the cation and the Ar atom to the center of the aromatic ring, represented by R and R', respectively, and the angle α formed by $\vec{R}$ and $\vec{R}'$ (Figure 1) are characterized. As indicated in the previous section, the total $M^+-C_6F_6$−Ar energy is decomposed in $M^+-C_6F_6$, Ar−C_6F_6, and M^+−Ar contributions, whose competition defines the geometry of the ternary compounds at equilibrium. To understand such interaction competition, the characteristics of the Ar−C_6F_6, $M^+-C_6F_6$, and Ar−M^+ binary compounds are first considered. For the Ar−C_6F_6 dimer, the minimum interaction energy corresponds to an equilibrium

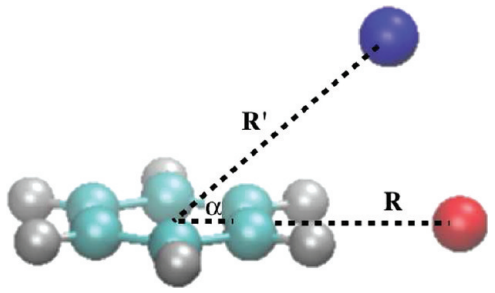

Figure 1. Geometry of the $M^+-C_6F_6$−Ar aggregates at the equilibrium configuration. M^+ and Ar are represented in red and blue colors respectively.

dx.doi.org/10.1021/jp300156k | J. Phys. Chem. A 2012, 116, 3094−3102

structure in which the Ar atom is placed along the C_6 rotational axis of C_6F_6 at 3.53 Å from its center of mass (c.m.), whereas that for $M^+-C_6F_6$ corresponds to a bifurcated structure, with the positive ion placed on the aromatic plane pointing to the center of a CC bond of the aromatic molecule, at a distance that depends on the ion mass.[26] As a matter of fact, the strength of the $M^+-C_6F_6$ interaction decreases with the mass of the ion, originating an increase of the equilibrium distance R (an enlargement of R of about 20% is observed when Na^+ is substituted by Cs^+). In the most stable structure of the ternary $M^+-C_6F_6-Ar$ aggregate, the equilibrium geometry of the $M^+-C_6F_6$ fragment is conserved, whereas that of the $Ar-C_6F_6$ one is not. Details of the particular geometry of the investigated ternary aggregates at the equilibrium are given in Table 3. As it

Table 3. Distance from the Center of Mass of C_6F_6 to the Ar Atom and to the Cation Represented by R and R', Respectively, and Angle (α) formed by the $\vec{R}$ and $\vec{R}'$ Vectors

$M^+-C_6F_6-Ar$	R/Å	R'/Å	α/deg
$Na^+-C_6F_6-Ar$	4.10	4.73	35.06
$K^+-C_6F_6-Ar$	4.48	4.51	41.41
$Rb^+-C_6F_6-Ar$	4.65	4.44	43.07
$Cs^+-C_6F_6-Ar$	4.88	4.37	45.44

can be seen, while R and α increase with the ion mass, R' decreases. The strength of the $Ar-M^+$ interaction also decreases with the ion mass and the Ar atom in the heavier aggregates tends to occupy a position closer to the C_6 axis of C_6F_6 than in the lightest ones. To better appreciate the differences in the geometry of the $M^+-C_6F_6-Ar$ systems, we have considered, at the equilibrium, the following energy contributions to the total potential energy (V_{cfg}): $Ar-M^+$ (V_{pair}), $Ar-C_6F_6$ ($V_{Ar-C_6F_6}$), and both the $M^+-C_6F_6$ electrostatic (V_{el}) and nonelectrostatic (V_{nel}) contributions ($V_{M^+-C_6F_6} = V_{el} + V_{nel}$), whose values are given in Table 4. As can be seen,

Table 4. M^+-Ar (V_{pair}), $Ar-C_6F_6$ ($V_{Ar-C_6F_6}$), and $M^+-C_6F_6$ ($V_{M^+-C_6F_6}$) Energy Contributions to the Total Potential Energy of the Equilibrium (Most Stable) Configuration (V_{cfg})[a]

$M^+-C_6F_6-Ar$	V_{cfg}/meV	V_{pair}/meV	$V_{Ar-C_6F_6}$/meV	V_{el}/meV	V_{nel}/meV
$Na^+-C_6F_6-Ar$	−704.94	−166.91	−28.44	−182.82	−326.77
$K^+-C_6F_6-Ar$	−531.34	−109.74	−31.45	−149.39	−240.76
$Rb^+-C_6F_6-Ar$	−486.11	−96.52	−31.92	−137.05	−220.62
$Cs^+-C_6F_6-Ar$	−443.53	−84.75	−32.84	−123.39	−202.55

[a] $V_{M^+-C_6F_6}$ is expressed in terms of its electrostatic (V_{el}) and nonelectrostatic (V_{nel}) components.

independently of the ion mass, V_{nel} is the most important energy contribution, representing about a 45% of V_{cfg}. As has been indicated, for the heavier aggregates, the Ar atom is placed closer to the rotational axis of C_6F_6 and farther from the ion than for the lightest ones. Accordingly, a decrease (more negative value) of $V_{Ar-C_6F_6}$ and an increase (less negative value) of V_{pair} are observed when the mass of the ion increases. Only small changes in the relative values of both V_{nel} and V_{el} with respect to V_{cfg} are predicted for the different ions. As a matter of fact, the $V_{M^+-C_6F_6}$ energy contribution is very close to that of the bare $M^+-C_6F_6$.[26] This finding gives support to the idea that, in presence of a high number of Ar atoms, the system can be considered as $M^+-C_6F_6$ (solute) solvated by Ar atoms (solvent).

4. MOLECULAR DYNAMICS RESULTS

To study the microsolvation process, some small clusters of the $M^+-C_6F_6-Ar_n$ type ($n \leq 30$) and the $M^+-C_6F_6$ aggregates solvated by ensembles of 50, 100, 200, and 485 Ar atoms have been considered. The small aggregates and the Ar solvation effects on the $M^+-C_6F_6$ systems, observed by increasing the number of Ar atoms, have been both investigated by means of MD simulations using the DL_POLY program.[57] The smaller aggregates ($n \leq 30$) have been investigated performing MD calculations for a fixed number of particles (N) in a given volume (V) ensuring the conservation of the energy (E) (NVE ensemble). The trajectories for a given aggregate have been run at increasing values of total (kinetic plus potential) energy, E_{total} (and of the temperature). To investigate possible volume variations at a given mean pressure (p) and temperature (T), a NpT ensemble of particles has been considered to study the heavier (n = 50, 150, 250, and 485) aggregates. The trajectories have been run at increasing values of T. The C_6F_6 molecule has been kept rigid in all calculations and the trajectories have been integrated along 15 ns, using a time step of 1 fs. Previously, the system has been equilibrated using the same time step for 0.1 ns. The equilibration period, during which the velocities of all atoms are rescaled, allows us to match the input temperature. The values of the positions and of the energy contributions obtained during the equilibrium period are excluded in the statistical analysis at the end of the trajectory. For a given value of n, the starting configuration has been constructed by randomly placing the Ar atoms around the $M^+-C_6F_6$ dimer in its minimum energy configuration and following the same procedure used before to investigate the Ar solvated $X^-C_6H_6$ aggregates.[42,46] To analyze the energy results, the mean value of the configuration energy, E_{cfg}, representing the average of the potential energy over all accessible configurations of the aggregate at the chosen E_{total}, has been partitioned in $E_{M^+-C_6F_6}$, $E_{Ar-C_6F_6}$, and E_{pairs}, associated to the $M^+-C_6F_6$, $Ar-C_6F_6$ and all pair interactions ($Ar-M^+$ and $Ar-Ar$), respectively.

4.1. Small $M^+-C_6F_6-Ar_n$ Aggregates ($n \leq 30$). The energetics of the solvated $M^+-C_6F_6$ aggregates has been investigated by performing calculations for the different systems surrounded by the same number of Ar atoms at a given temperature. Results obtained for the small clusters indicate that some properties are independent of the ion size. For instance $E_{M^+-C_6F_6}$ remains almost unaffected by increasing the number of Ar atoms, indicating that such an increase ($n \leq 30$) does not originate noticeable changes in the preferred geometry of the bare $M^+-C_6F_6$ aggregates. As a matter of fact, by increasing n from 1 to 30, the variation of $E_{M^+-C_6F_6}$ is in all cases lesser than 1%. Moreover, it has been also observed that Ar atoms tend to interact with both C_6F_6 and M^+ independently of the ion size. However, as the strength of the interaction decreases with the ion mass, the mobility of the Ar atoms is higher for the heavier systems, as can be seen in Figure 2 for $M^+-C_6F_6-Ar_2$. Due to the decrease of the M^+-Ar binding energy, which at the equilibrium configuration is equal to 167 meV for Na^+-Ar and to 85 meV for Cs^+-Ar, the competition between the $Ar-C_6F_6$ and the M^+-Ar interactions is higher for the heavier aggregates and the Ar atoms can occupy positions

dx.doi.org/10.1021/jp300156k | J. Phys. Chem. A 2012, 116, 3094−3102

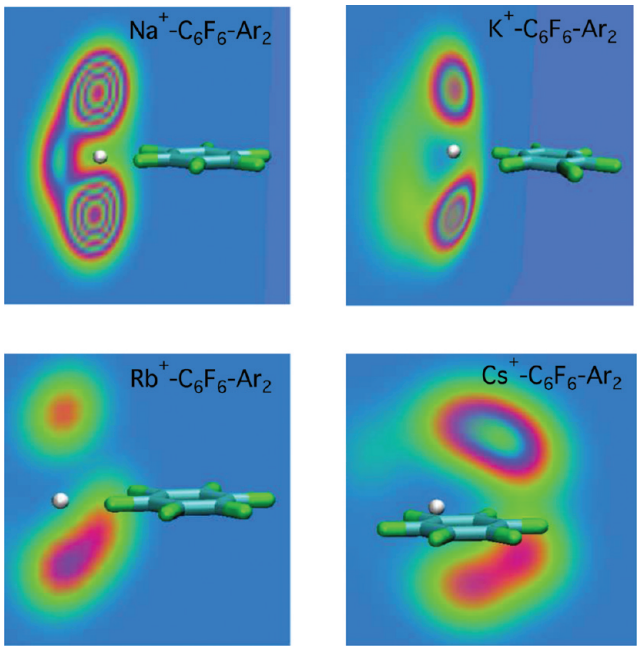

Figure 2. Two-dimensional maps of the probability density of two Ar atoms around the $M^+-C_6F_6$ aggregates. Results correspond to MD simulations at a temperature of 30 K. M^+ is represented in white.

closer to the rotational axis of the aromatic compound (not allowed for the lightest clusters). The two-dimensional representations of the density of probability shown in Figure 2, derived from volumetric data using the Volmap tool included in the VMD visualization program,[58] evidence the higher mobility of the two Ar atoms when the mass of the aggregate increases. As can be observed in the figure, the probability density is symmetric for the lightest aggregates, whereas it is not for the heaviest ones. This seems to indicate that in the $Na^+-C_6F_6-Ar_2$ and the $K^+-C_6F_6-Ar_2$ aggregates the Ar atoms tend to be placed in opposite sides of the aromatic ring, whereas a tendency to be placed on the same side of the C_6F_6 plane is observed for the $Rb^+-C_6F_6-Ar_2$ and the $Cs^+-C_6F_6-Ar_2$ systems. As a matter of fact, due to the decrease of both $E_{M^+-C_6F_6}$ and E_{M^+-Ar} with the ion size, the heavier aggregates form less compacted structures than the lightest ones, in which the cation and the Ar atoms are placed at larger distances from the C_6F_6 center of mass. This originates that the most stable structure for $Na^+-C_6F_6-Ar_2$ and $K^+-C_6F_6-Ar_2$ is the one in which the Ar atoms are placed in opposite sides of the aromatic plane. In these cases, due to the compactness of the structures, isomerization processes are unlikely. Thereby, the Ar atoms remain in opposite sides of the aromatic plane and, in these cases, the density of Ar atoms around $Na^+-C_6F_6$ and $K^+-C_6F_6$ (top panels of Figure 2) presents a high symmetry. On the contrary, for the heavier clusters, the larger $M^+-C_6F_6$ equilibrium distance allows us to obtain stabler structures with the two Ar atoms in the same side of the C_6F_6 molecular plane. In this case, the Ar–Ar interaction increases and the structure with two Ar atoms interacting between them is the most stable one. These structures are less compact and isomerization processes are likely to occur. Accordingly, the density of Ar atoms around $Rb^+-C_6F_6$ and $Cs^+-C_6F_6$ shown in the lower panels of Figure 2 do not present any symmetry.

With a further increase of *n*, it has been observed that the compactness of the structures formed by the Ar atoms surrounding $M^+-C_6F_6$ depends on the ion mass. The same behavior was observed in the Ar solvation of those aggregates that halides form with benzene.[46] Bearing in mind that the strength of the $M^+-C_6F_6$ interaction diminishes with the cation mass (originating an increase of the equilibrium distance from M^+ to the center of mass of C_6F_6), it can be understood that the Ar atoms solvating the heaviest aggregates can be placed closer to C_6F_6 than those solvating the lightest ones. For instance, an analysis of the geometry and energy of $M^+-C_6F_6-Ar_5$ aggregates allows us to see that $E_{Ar-C_6F_6}$ is lower (more negative) for the heavier aggregate, being equal to −75 meV, −85 meV, −88 meV and −101 meV for $Na^+-C_6F_6-Ar_5$, $K^+-C_6F_6-Ar_5$, $Rb^+-C_6F_6-Ar_5$ and $Cs^+-C_6F_6-Ar_5$, respectively. Moreover, the percentual contribution of E_{pairs} within E_{cfg} increases (less negative) with the ion mass. These results are in agreement with the three-dimensional probability density of the Ar atoms shown in Figure 3. The represented isosurfaces

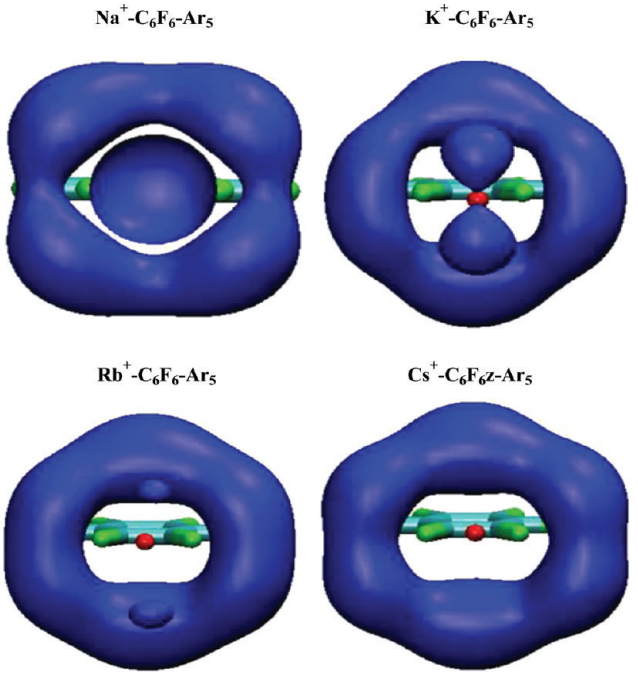

Figure 3. Isosurface (0.85) plot of the Ar probability density in the $M^+-C_6F_6-Ar_5$. Results correspond to MD simulations at a temperature of 30 K. M^+ is represented in red.

can be interpreted as Ar orbitals (see for instance refs 42, 46, and 48). As can be seen, for $Na^+-C_6F_6-Ar_5$ four Ar atoms interact with both C_6F_6 and Na^+ but the fifth atom is placed behind the cation. When the size of the ion increases, the Ar atoms are placed closer C_6F_6 but at larger distances from the cation. As can be seen in the top panel of Figure 4, the Ar atoms are placed at larger distances from the center of mass (c.m.) of C_6F_6 in the $Na^+-C_6F_6Ar_5$ aggregates than in the other ones. On the other hand, the Ar–Ar radial distribution functions (RDFs) show that the first peak appears approximately at the same distance, independently of the mass of the ion, whereas the second one occurs at larger distances for the heavier $M^+-C_6F_6$ aggregates (medium panel of Figure 4). Moreover, in the lower panel of the figure it can be seen that the heaviest cations are placed at larger distances from the C_6F_6 center of mass than the lightest ones.

dx.doi.org/10.1021/jp300156k | J. Phys. Chem. A 2012, 116, 3094–3102

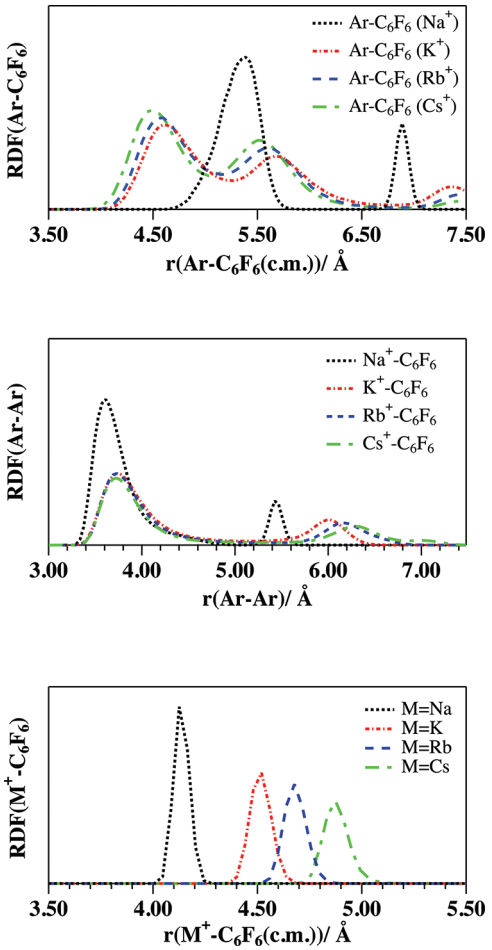

Figure 4. Ar−C_6F_6 (top panel), Ar−Ar (middle panel), and M^+−C_6F_6 (lower panel) radial distribution functions (RDFs) for the M^+−C_6F_6−Ar_5 aggregate. Results correspond to MD simulations at a temperature of 30 K.

The analysis of the energy contributions shows that, in general, $E_{Ar-C_6F_6}$ tends to become more negative with increasing n (see the lower panel of Figure 5) and this raises the global binding energy. However, due to the different interaction energy for approaches of Ar on the C_6F_6 plane in comparison with the perpendicular ones (Ar along the C_6 rotational axis of C_6F_6), noticeable fluctuations of $E_{Ar-C_6F_6}$ are observed. Bearing in mind that the probability for an isomerization process increases with n, the previous results are not surprising and should indicate that isomerizations are likely to occur for systems containing more than 8 Ar atoms. Accordingly, the variation of $E_{Ar-C_6F_6}$ by increasing n does not follow a regular trend. On the contrary, no fluctuations on E_{pairs} are observed when n increases. This behavior can be explained considering that both the Ar−Ar and the M^+−Ar interactions, included in E_{pairs}, only exhibit a radial dependence. The analysis of the results indicates that, for a given value of n, the probability of isomerization depends on the initial configuration and on the size of the cation. For this reason, similar initial configurations have been considered to investigate the role of the ion size in M^+−C_6F_6−Ar_n systems. Results show that the *magic* numbers that complete groups of Ar atoms showing a particular spatial disposition around the ionic M^+−C_6F_6 dimers, as was observed for anion−benzene systems,[46] depend on the ion. For instance, as it can be observed in Figure 6, n = 10 is *magic* for Cs^+−C_6F_6

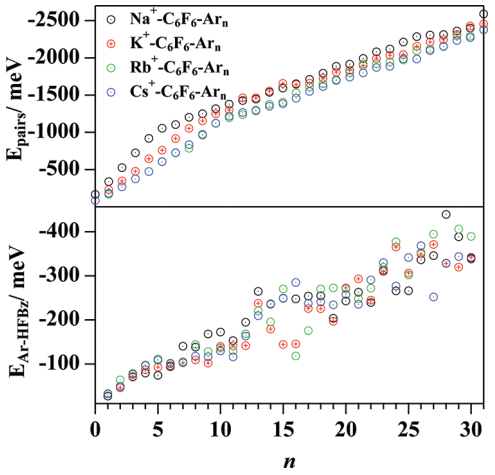

Figure 5. Mean Ar−C_6F_6 energy, $E_{Ar-C_6F_6}$, and mean pair energy contributions (including ion−Ar and Ar−Ar), E_{pairs}, represented as a function of the number of Ar atoms in the lower and the top panels, respectively. Results correspond to MD simulations at a temperature of 30 K.

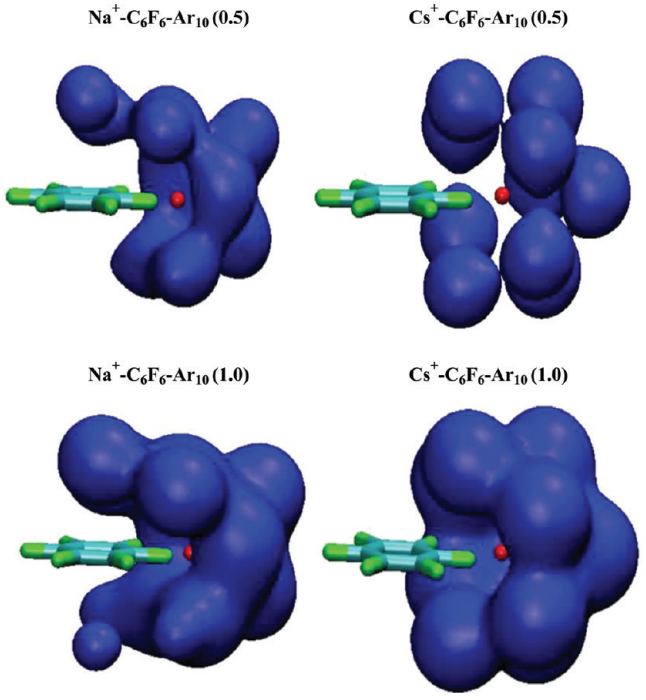

Figure 6. Isosurface plots of the Ar probability density for the Na^+−C_6F_6−Ar_{10} (on the left-hand side) and for the Cs^+−C_6F_6−Ar_{10} at two different isovalues indicated in the figure. Results correspond to MD simulations at a temperature of 30 K. M^+ is represented in red.

(right-hand side) but it is not for Na^+−C_6F_6 (left-hand side). As a matter of fact, 10 Ar atoms cannot form compact structures around Na^+−C_6F_6 and in such case some Ar atoms present a high mobility, which favors the isomerization processes. On the contrary, the same number of Ar atoms are able to form very compact structures around Cs^+−C_6F_6 and, accordingly, here the Ar atoms tend to occupy fixed positions. In the latter case, the isomerization processes are unlikely to occur.

4.2. From Cluster Rearrangement to Solvation Dynamics. To investigate the evolution from cluster rearrangement to solvation dynamics, the M^+−C_6F_6 aggregates

dx.doi.org/10.1021/jp300156k | J. Phys. Chem. A 2012, 116, 3094−3102

have been solvated by ensembles of 50, 150, 250, and 485 Ar atoms. The simulations have been performed at constant values of the mean temperature and pressure. The temperature effect has been investigated running trajectories at increasing values of T.

At low temperatures, the Ar spatial distribution for $M^+-C_6F_6$ solvated by 50 Ar atoms does not depend on the ion size. As was observed for the $K^+-C_6F_6-Ar_n$ systems,[48] the Ar atoms tend to be placed close to the cation, as can be deduced from Figure 7. Moreover, the geometry of the solvated $M^+-C_6F_6$ and

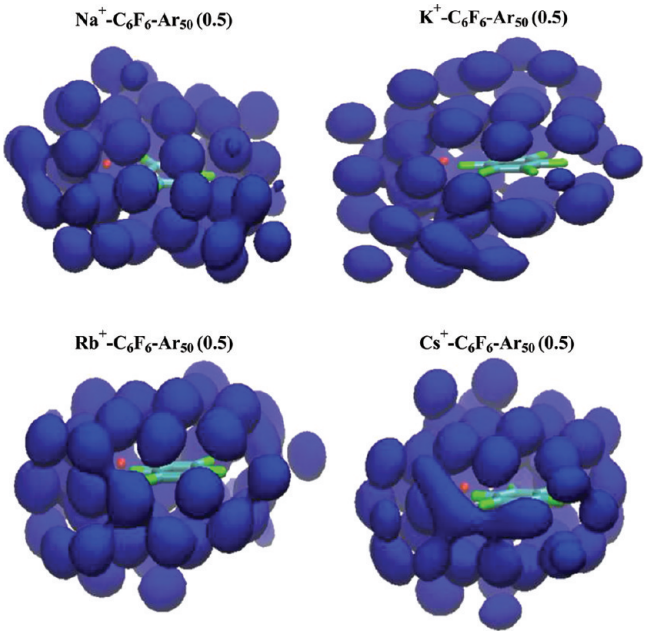

Figure 7. Isosurface plots of the Ar probability density for the $M^+-C_6F_6$ aggregates solvated by 50 Ar atoms at the isovalue 0.5. Results correspond to MD simulations at a temperature of 80 K.

that of the bare $M^+-C_6F_6$ system are very similar. In particular, at temperature values close to 80 K, the distance from the cation to the center of the aromatic ring is only about a 2% larger than the corresponding unsolvated systems. At higher temperatures, in spite of the fact that the increase of T originates frequent variations on the spatial distribution of the Ar atoms, the volume of the system remains nearly constant. This behavior contrasts with that observed for larger systems ($n \geq 150$).

At low temperatures, when $M^+-C_6F_6$ is solvated by a number of Ar atoms ≥150, the distance from the cation to the center of the aromatic ring is about a 6% larger than the corresponding distance in the unsolvated $M^+-C_6F_6$, thus facilitating the complete solvation of M^+.[47] Due to the enlargement of the distance from M^+ to C_6F_6, the M^+-Ar RDFs look different than those observed for the small $M^+-C_6F_6-Ar_n$ aggregates. In Figure 8, the M^+-Ar radial distribution functions derived from MD simulations at 110 K are presented. As can be seen in the figure, the first peak of the RDFs appears, independently of the ion size, at a value close to the equilibrium distances of the M^+-Ar dimers (Table 2), which are shorter than those obtained previously for the small aggregates. Moreover, at temperature values close to 120 K, a sudden expansion of the Ar atoms occurs. As a matter of fact, at 120 K important changes in both the density values and diffusion coefficients are also observed for a system composed

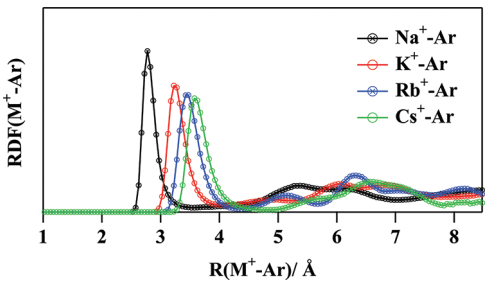

Figure 8. M^+-Ar radial distribution functions (RDFs) for the $M^+-C_6F_6$ aggregates solvated by 250 Ar atoms. Results correspond to MD simulations at a temperature of 110 K.

of 500 Ar atoms.[47] The expansion process observed for the $M^+-C_6F_6$ solvated systems does not take place exactly at the same temperature for all aggregates and it is observed at lower temperatures for the lightest systems. This behavior can be attributed to the higher $Ar-Na^+$ interaction energy in comparison with the corresponding one for the heavier ions. At a given T, for a number of Ar atoms high enough, the $Ar-M^+$ energy contribution is able to break the attraction of the ion with the aromatic molecule. In spite of the fact that the lightest $M^+-C_6F_6$ aggregates are stabler that the heaviest ones, the $Ar-M^+$ contribution allows an easier $M^+-C_6F_6$ dissociation for the lightest $Na^+-C_6F_6$ aggregate. The clouds formed by 485 Ar atoms at T = 115 K, are represented in Figure 9, where it can be seen the dissociation of the $Na^+-C_6F_6$. At the same conditions, the remaining aggregates does not dissociate. The energy needed to release M^+ from C_6F_6 is compensated by the increase of the $Ar-C_6F_6$ and $M^+-C_6F_6$ energy contributions and the

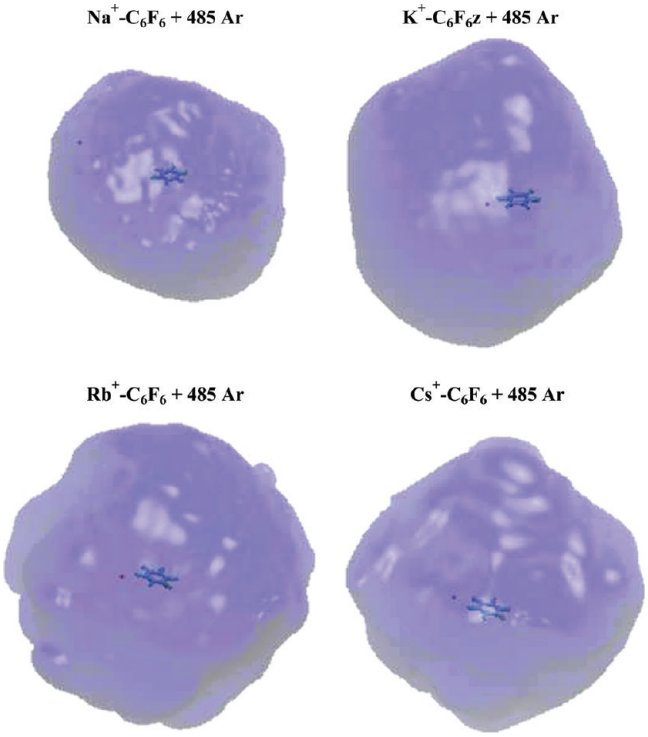

Figure 9. Isosurface plots of the Ar probability density for the $M^+-C_6F_6$ aggregates solvated by 485 Ar atoms at the isovalue 0.3. On the top and on the left-hand side it can be seen the dissociation of the $Na^+-C_6F_6$ aggregate. Results correspond to MD simulations at a temperature of 115 K.

dx.doi.org/10.1021/jp300156k | J. Phys. Chem. A 2012, 116, 3094−3102

corresponding energy difference defines the enthalpy change of the solution.

5. CONCLUDING REMARKS

The dynamics of the alkali metal ion−C_6F_6 systems surrounded by a different number of Ar atoms have been investigated from molecular dynamics simulations using an analytical potential energy function described as a sum of two-body, three-body nonelectrostatic and electrostatic contributions. The first two contributions have been represented using an ILJ function, whereas the electrostatic ones have been evaluated as a sum of Coulomb interactions between the charge of cations and a charge distribution on C_6F_6 compatible with its quadruple moment. The microscopic characteristics of the Ar solvation process have been investigated by considering the M^+−C_6F_6 system surrounded by a different number of atoms. Results of the study of small M^+−C_6F_6−Ar_n aggregates ($n \leq 30$) indicate that the M^+−C_6F_6 remains almost unaffected, independently of the cation mass, by increasing the number of Ar atoms, even at the highest temperature values investigated. With increasing T, the mobility of the Ar atoms also increases, and due to the decrease of the Ar−M^+ pair binding interaction with the ion mass, the mobility of the Ar atoms and, accordingly, the probability of isomerization increase with the ion mass. Some differences on the aggregates behavior have been attributed to the nature of the ion. As a matter of fact, bigger ions exhibit weaker interactions with both Ar and C_6F_6, which determines different equilibrium structures and different mobilities of the Ar atoms in the M^+−C_6F_6−Ar_n aggregates. The different strengths of the Ar−M^+ interaction, depending on the cation, originate different magic numbers of Ar atoms forming the first compact structure in the M^+−C_6F_6−Ar_n aggregate. Upon a further increase of the number of Ar atoms, the observation of microscopic aspects at the atomic level is difficult; however, some more macroscopic aspects are manifested. In particular, the radial distribution functions with the first peak at short distances indicate the solvation of the M^+ ion, which, once solvated, can fly away from C_6F_6.

AUTHOR INFORMATION

Corresponding Author

*E-mail: m.alberti@ub.edu.

Notes

The authors declare no competing financial interest.

ACKNOWLEDGMENTS

M.A. acknowledges financial support from the Ministerio de Educación y Ciencia (Spain, Projects CTQ2010-16709 and PR2010-0243) and to the Comissionat per a Universitats i Recerca del DIUE (Generalitat de Catalunya, Project 2009-SGR 17). Also thanks are due to the Centre de Serveis Científics i Acadèmics de Catalunya CESCA and Fundació Catalana per a la Recerca for the allocated supercomputing time. N.F.L. acknowledges MIUR PRIN 2008 contract 2008KJX4SN_003, Phys4entry FP7/2007-2013 contract 242311 and CASPUR for the allocated computing time.

REFERENCES

(1) Meyer, E. A.; Castellano, R. K.; Diederich, F. *Angew. Chem., Int. Ed.* **2003**, *42*, 1210.
(2) Sa, R.; Zhu, W.; Shen, J.; Gong, Z.; Cheng, J.; Chen, K.; Jiang, H. *J. Phys. Chem. B* **2006**, *110*, 5094.
(3) Kim, D.; Hu, S.; Tarakeshwar, P.; Kim, S. K. *J. Phys. Chem. A* **2003**, *107*, 1228.
(4) Nicholas, J. B.; Hay, B. P.; Dixon, D. A. *J. Phys. Chem. A* **1999**, *103*, 1394.
(5) Tsuzuki, S.; Yoshida, M.; Uchimaru, T.; Mikami, M. *J. Phys. Chem. A* **2001**, *105*, 769.
(6) Cubero, E.; Luque, F. J.; Orozco, M. *Proc. Natl. Acad. Sci. U. S. A.* **1998**, *95*, 5976.
(7) Cubero, E.; Orozco, M.; Luque, F. J. *J. Phys. Chem. A* **1999**, *103*, 315.
(8) Soteras, I.; Orozco, M.; Luque, F. J. *Phys. Chem. Chem. Phys.* **2008**, *10*, 2616.
(9) Coletti, C.; Re, N. *J. Phys. Chem. A* **2006**, *110*, 6563.
(10) Albertí, M.; Aguilar, A.; Lucas, J. M.; Pirani, F.; Cappelletti, D.; Coletti, C.; Re, N. *J. Phys. Chem. A* **2006**, *110*, 9002.
(11) Ma, J. C.; Dougherty, D. A. *Chem. Rev.* **1997**, *97*, 1303.
(12) Kumpf, R. A.; Dougherty, D. A. *Science* **1993**, *261*, 1708.
(13) Dougherty, D. A. *Science* **1996**, *271*, 163.
(14) Quiñonero, D.; Garau, C.; Rotger, M. C.; Frontera, A.; Ballester, P.; Costa, A.; Deyà, P. M. *Angew. Chem., Int. Ed.* **2002**, *41*, 3389.
(15) Garau, C.; Frontera, A.; Quiñonero, D.; Ballester, P.; Costa, A.; Deyà, P. M. *Chem. Phys. Chem.* **2003**, *4*, 1344.
(16) Garau, C.; Frontera, A.; Quiñonero, D.; Ballester, P.; Costa, A.; Deyà, P. M. *Chem. Phys. Lett.* **2003**, *382*, 534.
(17) Garau, C.; Frontera, A.; Quiñonero, D.; Ballester, P.; Costa, A.; Deyà, P. M. *New J. Chem.* **2003**, *27*, 211.
(18) Garau, C.; Quiñonero, D.; Frontera, A.; Escudero, D.; Ballester, P.; Costa, A.; Deyà, P. M. *Chem. Phys. Lett.* **2007**, *438*, 104.
(19) Estarellas, C.; Rotger, M. C.; Capó, M.; Quiñonero, D.; Frontera, A.; Costa, A.; Deyà., P. M. *Org. Lett.* **2009**, *11*, 1987.
(20) Escudero, D.; Frontera, A.; Quiñonero, D.; Deyà., P. M. *Chem. Phys. Lett.* **2008**, *455*, 325.
(21) Coletti, C.; Re, N. *J. Phys. Chem. A* **2009**, *113*, 1578.
(22) Albertí, M.; Aguilar, A.; Lucas, J. M.; Pirani, F.; Coletti, C.; Re, N. *J. Phys. Chem. A* **2009**, *113*, 14606.
(23) Kim, D.; Tarakeshwar, P.; Kim, S. K. *J. Phys. Chem. A* **2004**, *108*, 1250.
(24) Schottel, B. L.; Chifotides, H. T.; Dunbar, K. R. *Chem. Soc. Rev.* **2008**, *37*, 68.
(25) Garau, C.; Frontera, A.; Quiñonero, D.; Ballester, P.; Costa, A.; Deyà, P. M. *J. Phys. Chem. A* **2004**, *108*, 9423.
(26) Albertí, M.; Aguilar, A.; Lucas, J. M.; Pirani, F. *J. Phys. Chem. A* **2010**, *114*, 11964.
(27) Albertí, M.; Castro, A.; Laganà, A.; Moix., M; Pirani, F.; Cappelletti, D. *Eur. Phys. J. D* **2006**, *38*, 185.
(28) Albertí, M.; Pacifici, L.; Laganà, A.; Aguilar, A. *Chem. Phys.* **2006**, *327*, 105.
(29) Garau, C.; Frontera, A.; Quiñonero, D.; Ballester, P.; Costa, A.; Deyà, P. M. *Chem. Phys. Lett.* **2004**, *392*, 85.
(30) Quiñonero, D.; Garau, C.; Frontera, A.; Ballester, P.; Costa, A.; Deyà, P. M. *J. Phys. Chem. A* **2005**, *109*, 4632.
(31) Quiñonero, D.; Frontera, A.; Garau, C.; Ballester, P.; Costa, A.; Deyà, P. M. *ChemPhysChem* **2006**, *7*, 2487.
(32) Rodríguez-Otero, J.; Cabaleiro-Lago, E.; Peña-Gallego, A. *Chem. Phys. Lett.* **2008**, *452*, 49.
(33) Cabarcos, O. M.; Weinheimer, J. C.; Lisy, J. M. *J. Chem. Phys.* **1999**, *110*, 8429.
(34) Otashi, H.; Radnai, T. *Chem. Rev.* **1993**, *93*, 1157.
(35) Impey, R. W.; Madden, P. A.; McDonald, I. R. *J. Phys. Chem.* **1983**, *87*, 5071.
(36) *Ionic Hydration in Chemistry and Biophysics*; Studies in Physical and Theoretical Chemistry 12; Conway, B. E., Ed.; Elsevier: Amsterdam, 1981.
(37) *Ion solvation*; Marcus, Y., Ed.; Wiley: Chichester, U.K., 1986.
(38) Leutwyler, S.; Jortner, J. *J. Phys. Chem.* **1987**, *91*, 5558.
(39) Leutwyler, S.; Bösiger, J. *Chem. Rev.* **1990**, *90*, 489.
(40) Douin, S.; Parneix, P.; Amar, F. G.; Bréchignac, Ph. *J. Phys. Chem. A* **1997**, *101*, 122.
(41) Amirav, A.; Even, U.; Jortner, J. *J. Chem. Phys.* **1981**, *75*, 2489.

(42) Huarte-Larrañaga, F.; Aguilar, A.; Lucas, J. M.; Albertí, M. *Theor. Chem. Acc.* **2011**, *128*, 757.
(43) Albertí, M.; Aguilar, A.; Lucas, J. M.; Laganà, A.; Pirani, F. *J. Phys. Chem. A* **2007**, *111*, 1780.
(44) Huarte-Larrañaga, F.; Aguilar, A.; Lucas, J. M.; Albertí, M. *J. Phys. Chem. A* **2007**, *111*, 8072.
(45) Albertí, M.; Aguilar, A.; Lucas, J. M.; Pirani, F. *Theor. Chem. Acc.* **2009**, *123*, 21.
(46) Albertí, M.; Huarte-Larrañaga, F.; Aguilar, A.; Lucas, J. M.; Pirani, F. *Phys. Chem. Chem. Phys.* **2011**, *13*, 8251.
(47) Albertí, M.; Pirani, F. *J. Phys. Chem. A* **2011**, *115*, 6394.
(48) Albertí, M.; Faginas Lago, N.; Pirani, F. *J. Phys. Chem. A* **2011**, *115*, 10871.
(49) Cambi, R.; Cappelletti, D.; Liuti, G.; Pirani, F. *J. Chem. Phys.* **1991**, *95*, 1852.
(50) Pirani, F.; Cappelletti, D.; Liuti, G. *Chem. Phys. Lett.* **2001**, *350*, 286.
(51) Faginas Lago, N.; Huarte Larrañaga, F.; Albertí, M. *Eur. Phys. J. D* **2009**, *55*, 75.
(52) Pirani, P.; Brizi, S.; Roncaratti, L. F.; Casavecchia, P.; Cappelletti, D.; Vecchiocattivi, F. *Phys. Chem. Chem. Phys.* **2008**, *10*, 5489.
(53) Albertí, M.; Faginas Lago, N.; Pirani, F. *Chem. Phys.* **2011**, DOI: 10.1016/j.chemphys.2011.08.009.
(54) Denbigh, K. G. *Trans. Faraday Soc.* **1940**, *36*, 936.
(55) Albertí, M.; Faginas Lago, N.; Laganà, A.; Pirani, F. *Phys. Chem. Chem. Phys.* **2011**, *13*, 8422.
(56) Albertí, M.; Aguilar, A.; Pirani, F. *J. Phys. Chem. A* **2009**, *113*, 14741.
(57) http://www.cse.scitech.ac.uk/ccg/software/DL_POLY/.
(58) Humphrey, W.; Dalke, A.; Schulten, K. VMD-Visual Molecular Dynamics. *J. Mol. Graph.* **1996**, *14*, 33.